

# Interfacial Decomposition Behaviour of Triethyl Phosphate-Based Electrolytes for Lithium-Ion Batteries

Florian Gebert,<sup>[a]</sup> Robin Lundström,<sup>[a]</sup> Wessel van Ekeren,<sup>[a]</sup> and Andrew J. Naylor<sup>\*[a]</sup>

Triethyl phosphate (TEP) is a cheap, environmentally benign, and non-flammable electrolyte solvent, whose implementation in lithium-ion batteries is held back by its co-intercalation into graphite anodes, resulting in exfoliation of the graphite structure. In this work, the electrode-electrolyte interface behaviour of electrolytes containing up to 100% TEP is investigated and correlated to electrochemical performance. High capacity and stable cycling are maintained with up to 30% TEP in carbonate ester-based electrolytes, but above this threshold the reversibility of  $\text{Li}^+$  intercalation into graphite drops sharply to almost zero. This represents a potential route to improved battery safety, while TEP can also improve safety

indirectly by enabling the use of lithium bis(oxalato)borate, a fluorine-free salt with limited solubility in traditional electrolytes. To understand the poor performance at TEP concentrations of  $>30\%$ , its solvation behaviour and interfacial reaction chemistry were studied. Nuclear magnetic resonance spectroscopy data confirms changes in the  $\text{Li}^+$  solvation shell above 30% TEP, while *operando* gas analysis indicates extensive gas evolution from TEP decomposition at the electrode above the threshold concentration, which is almost entirely absent below it. X-ray photoelectron spectroscopy depth profiling of electrodes demonstrates poor passivation by the solid electrolyte interphase above 30% TEP and significant graphite exfoliation.

## Introduction

The safety of lithium-ion batteries (LIBs), especially those used in electric vehicles, is becoming an increasingly prominent issue. LIBs have an overall good safety record in consumer applications. However, battery fires, even if they are rare, often become high-profile events, potentially undermining consumer confidence in the technology and the feasibility of the green transition. In addition, safety measures in commercial LIBs have to date typically involved engineering solutions, for example via thermal management systems<sup>[1]</sup> or using a safer but lower-energy cathode chemistry like lithium iron phosphate (LFP).<sup>[2]</sup> Such measures, while effective, inherently cut into energy density.

Battery safety is a multifaceted concept that covers thermal, chemical, and electrical safety, but the thermal and chemical aspects are particularly important at the cell level,<sup>[3]</sup> where materials properties are decisive. Thermal and chemical safety are closely related: a battery fire can destroy the cell packaging, causing toxic components to leak. While a number of battery components are flammable, including the packaging, electrode materials and separators, the electrolyte is usually the most flammable component and the proximate cause of thermal runaway. For this reason, it is of great interest to develop

electrolytes that are both low-toxicity and non-flammable. Unfortunately, these goals are often at odds with one another: the most viable non-flammable electrolytes are highly fluorinated compounds.<sup>[4]</sup> The main alternatives – other than solid electrolytes, which are promising but face unresolved issues around manufacturability<sup>[5,6]</sup> and interfacial resistance;<sup>[7]</sup> and ionic liquids, which are limited by their cost and viscosity<sup>[8]</sup> – are organophosphates. Phosphorus-containing compounds are excellent radical scavengers. Their presence can slow or even stop the radical propagation reactions that comprise combustion processes.<sup>[9]</sup> Because of the high viscosities of phosphates with long alkyl chains, research has focused on the two simplest phosphates, trimethyl phosphate (TMP) and triethyl phosphate (TEP). However, these phosphates come with a significant trade-off: their strong solvation of  $\text{Li}^+$  causes them to co-intercalate into graphite, which leads to the continuous decomposition of the solvent and exfoliation of the graphite structure.<sup>[10,11]</sup>

Graphite-based cells containing TEP invariably use low TEP contents of 5–30% to achieve stable cycling.<sup>[12–15]</sup> However, there has to date been no systematic investigation into why low TEP contents are stable and higher ones are not. Zeng et al. recently demonstrated that stable cycling can also be achieved by significantly increasing the salt concentration. The authors of that study hypothesized that the ratio of lithium ions to TEP molecules in an electrolyte is decisive for its electrochemical stability. Specifically, it was proposed that the coordination of TEP by  $\text{Li}^+$  reduces its reactivity and prevents its decomposition, with an optimal  $\text{Li}^+:\text{TEP}$  ratio suggested to be 0.5 (corresponding to ca. 3 mol L<sup>-1</sup> in pure TEP).<sup>[16]</sup>

Here, we investigate the behaviour of electrolytes with varying TEP content in combination with co-solvents whilst fixing the  $\text{Li}^+$  concentration at 1 mol L<sup>-1</sup> for greater practical and commercial relevance. The electrochemical behaviour of

[a] F. Gebert, R. Lundström, W. van Ekeren, A. J. Naylor  
Department of Chemistry – Ångström Laboratory, Uppsala University, SE-75121 Uppsala, Sweden

E-mail: andy.naylor@kemi.uu.se

 Supporting information for this article is available on the WWW under <https://doi.org/10.1002/batt.202400342>

 © 2024 The Authors. *Batteries & Supercaps* published by Wiley-VCH GmbH. This is an open access article under the terms of the Creative Commons Attribution License, which permits use, distribution and reproduction in any medium, provided the original work is properly cited.

the TEP-containing electrolytes is tested in commercially-relevant NMC622 ( $\text{LiNi}_{0.6}\text{Mn}_{0.2}\text{Co}_{0.2}\text{O}_2$ )|graphite cells. Our results are consistent with recent work by Liu et al., which also explored the limits of usable TEP content in moderately concentrated carbonate ester-based electrolytes.<sup>[17]</sup> In the present work, the focus is placed on the study of interfacial reactions of these electrolytes with graphite electrodes. Nuclear magnetic resonance (NMR) spectroscopy confirms significant changes in  $\text{Li}^+$  solvation behaviour when varying the TEP content, while *operando* gas analysis gives insight into the degree of solvent decomposition during battery cycling. X-ray photoelectron spectroscopy (XPS) depth profiling reveals considerable differences in the composition of the solid electrolyte interphase (SEI) on graphite formed by the tested electrolytes. We also exploit an overlooked advantage of TEP: its high polarity allows it to solvate lithium bis(oxalato)borate (LiBOB) at the required concentrations. LiBOB is a fluorine-free electrolyte salt often cited as a less toxic and more environmentally friendly alternative to  $\text{LiPF}_6$ , but is held back, in part, by its poor solubility in most conventional carbonate ester-based solvents. In all, five electrolytes are studied, with TEP concentrations of 0%, 30%, 40%, 50% and 100% by volume, using a 3:7 (v/v) mixture of ethylene carbonate (EMC) and diethyl carbonate (DEC) as the base solvent and LiBOB as the salt.

## Experimental Section

### Materials

Electrolytes were prepared in an argon-filled glove box. TEP (99.8%, Sigma Aldrich) and EC:EMC (Solvionic) were combined in the required proportions and dried with molecular sieves (4 Å, Sigma Aldrich) for at least 72 hours. 1 M  $\text{LiPF}_6$  (99.9%, Sigma Aldrich) or LiBOB (Solvionic) was added and the mixture was stirred until the salt was fully dissolved. For the 100 vol% EC:EMC/0 vol% TEP electrolyte, a LiBOB concentration of 0.7 M was used due to solubility limitations. For the OEMS experiments, EC:DEC was used instead of EC:EMC, due to the simpler fragmentation spectrum of DEC.

2025 coin cells for electrochemical tests were assembled in an argon-filled glove box. Glass fiber (GF-A, Whatman) was used as the separator. For the XPS samples, an additional layer of Celgard 2500 separator was placed on the side facing the graphite anode to prevent adhesion of the glass fiber to the graphite surface. Circular discs 13 mm in diameter were cut from NMC622 coated on Al (2.0  $\text{mA h cm}^{-2}$ , Custom Cells) and graphite coated on Cu (2.4  $\text{mA h cm}^{-2}$ , Custom Cells) and dried in vacuum at 120 °C for 12 hours.

### Electrochemical Characterization

All cells were cycled at room temperature and rested for 10 hours after assembly. All cells, except those for the XPS, were subjected to two initial charge-discharge cycles at C/10 (based on a capacity of 2.65 mAh, which corresponds to a cathode specific capacity of 180  $\text{mA h g}^{-1}$ ) to ensure complete SEI formation. Long-term cycling tests were carried out at C/5. Cell resistance was measured using intermittent current interruption (ICI) experiments according to the protocol by Lacey et al.<sup>[18,19]</sup> Briefly, cells were cycled at C/5; the current was paused for 1 second every 5 minutes. From the voltage

drop at the end of the 1-second interruptions, the cell resistance was calculated via:

$$R_{cell} = -\frac{\Delta V_{1s}}{I}$$

where  $\Delta V_{1s}$  is the voltage drop and  $I$  is the current.

### X-Ray Photoelectron Spectroscopy (XPS)

Samples were prepared at the home laboratory by charging NMC622|graphite full cells and cycling them at C/10 until they reached their desired state of charge. In a glove box, the graphite electrode samples were extracted from cells, washed using EMC (for the EMC-containing cells) or TEP (for the EMC-free cells) to remove electrolyte residues, and dried under vacuum at room temperature for 1 hour. Samples were mounted on copper plates using conductive carbon tape. The sample plates were vacuum sealed and transported to the Surface and Interface Structural Analysis beamline (I09) at Diamond Light Source (Oxfordshire, UK). A transfer arm was used to move the air-sensitive samples between an argon glovebox and the beamline end-station.

Photoelectron spectra were recorded for the core level transitions using three different photon energies. Hard X-ray photoelectron spectroscopy (HAXPES) was performed using photon energies of 2350 and 7050 eV, monochromatized by a Si(111) double-crystal monochromator. Soft X-ray photoelectron spectroscopy (SOXPES) measurements were made at photon energies for each core level corresponding to a kinetic energy of 200 eV on a branch of the beamline that uses a plane grating monochromator. The beam was spread out using defocused settings to minimize radiation damage; the spot at the sample is estimated to be approximately 300 µm (H) and up to 1 mm (W). No charge neutralizer was used during the measurements. A hemispherical VG Scienta EW4000 analyser set to a pass energy of 70 eV for soft X-rays, and 200 eV for hard X-rays, was used to record spectra. The software package CasaXPS was used for analysis of photoelectron spectroscopy data and plots were generated using an in-house Python script. The spectra were calibrated to the peak corresponding to graphite (284 eV). The probing depth (3×IMFP – inelastic mean free path of electrons) for the HAXPES measurement at the excitation energy used was calculated using the TPP–M2 equation as detailed in the NIST database,<sup>[20]</sup> using parameters for polyethylene,<sup>[21]</sup> as a low-density material representative of the surface layer studied here.

### Online Electrochemical Mass Spectroscopy (OEMS)

A dedicated electrochemical gas cell was used for all OEMS experiments. The electrode stack comprised a Ø 13 mm NMC622 electrode in the bottom of the cell, followed by a Ø 16 mm glass fibre separator and finally a Ø 13 mm graphite electrode closest to the cell headspace. The electrode stack was soaked in 100 µL of LiBOB in EC:DEC + 30–100% TEP. The salt concentration was 1 M for the 30–100% TEP electrolytes and 0.7 M for the 0% TEP electrolyte. The electrode stack in the 0% TEP cell was soaked in 100 µL 0.7 M LiBOB EC:DEC. To facilitate gas diffusion from the electrodes to the headspace, the graphite electrode had Ø 0.01 mm holes, 6.4 holes/mm, laserered across the surface using a 5 W laser marking system (Östling, AIO G + 532 nm) using 35 passes and 70% laser power per hole. Any loose particles were removed by blowing  $\text{N}_2$  gas over the surface before drying the electrode in a Buchi oven at 120 °C for 12 h.

The cells were rested for 5 h after connecting to the OEMS to ensure a stable electrolyte background and temperature of 30 °C. The cells were cycled at C/10 rate for two cycles. Gas was purged and analysed every 10 min by the mass spectrometer during the OEMS experiments. The OEMS instrument was calibrated with H<sub>2</sub>, CH<sub>4</sub>, C<sub>2</sub>H<sub>4</sub>, O<sub>2</sub>, and CO<sub>2</sub> calibration gases prior to the experiment series. The OEMS instrument has previously been described by Lundström and Berg.<sup>[22]</sup>

### Nuclear Magnetic Resonance (NMR)

The NMR spectra of the neat TEP solvent and electrolyte mixtures were recorded on a 400 MHz JEOL ECZ spectrometer. Anhydrous deuterated dimethyl sulfoxide (DMSO-d<sub>6</sub>) (99.9%) from VWR was used as the solvent and was dried with molecular sieves prior to use. To prepare the NMR samples, an outer borosilicate tube (5 mm) was filled with the DMSO-d<sub>6</sub> reference. An inner fluorinated ethylene polypropylene (FEP) sample tube liner (3 mm) was filled with the neat solvent or electrolyte to prevent interactions between the reference solvent and the electrolyte samples. Both tubes were closed with poly(tetrafluoroethylene) (PTFE) plugs. All NMR samples were prepared in an argon-filled glovebox (O<sub>2</sub> < 1 ppm and H<sub>2</sub>O < 1 ppm). <sup>7</sup>Li-NMR, <sup>13</sup>C-NMR, and <sup>31</sup>P-NMR spectra were recorded.

## Results and Discussion

### Electrochemical Characterisation

Electrolytes were prepared with TEP and 3:7 v/v EC:EMC in varying volume ratios from 1:0 to 0:1. Lithium salts (LiBOB and LiPF<sub>6</sub>) were kept at a constant concentration of 1 M, except LiBOB in 100% EC:EMC, which was prepared at 0.7 M due to its poor solubility. NMC622|graphite cells were then cycled with these different electrolytes. Most noticeably, the discharge capacity decreases sharply when the TEP content exceeds 30 vol% (Figure 1a,b). Below this threshold, the capacity is not only high but very stable; the initial cell resistance is not increased by the presence of 30% TEP (Figure S1), despite a higher viscosity of TEP (1.8 mPas at 20 °C)<sup>[23]</sup> than EC:EMC (1.1 mPas).<sup>[24]</sup> The drop-off of capacity is observed irrespective

of the electrolyte salt used, although LiBOB displayed better long-term cycling performance (Figure 1c) and higher initial coulombic efficiency (Figure S2a). For this reason, and because of LiBOB's environmental and cost advantages, the remainder of the study investigates electrolyte formulations exclusively with LiBOB.

The fact that the decrease in reversible capacity is sudden, not gradual, implies the reactivity of the electrolyte also changes suddenly at the threshold TEP concentration of 30%. The near-zero 1<sup>st</sup>-cycle coulombic efficiency of these cells (Figure S2b) is consistent with the previously reported exfoliation of graphite by TEP,<sup>[11]</sup> with such a process known to result in disintegration of the electrode.<sup>[25]</sup> The threshold TEP content of 30%, which corresponds to a TEP:Li<sup>+</sup> ratio of ca. 1.8, is also roughly consistent with the previous reports by Zeng et al.,<sup>[16]</sup> in which TEP-containing electrolytes were stabilized by high lithium salt concentrations, and Liu et al.<sup>[17]</sup>

Cyclic voltammograms (CV) of graphite|Li cells containing these five electrolytes (Figure S3) similarly show fully reversible Li<sup>+</sup> intercalation and de-intercalation for the 0% and 30% TEP electrolytes, while no Li<sup>+</sup> de-intercalation at all is visible for the higher TEP concentrations. Interestingly, the onset potential of LiBOB reduction<sup>[26]</sup> remains constant at ca. 1.8 V vs. Li<sup>+</sup>/Li but the process overall becomes considerably more complex: the associated CV peak becomes broader and splits into two, starting at 40% TEP. In the electrolytes containing 40% TEP and above, a broad peak beginning at 0.8 V vs. Li<sup>+</sup>/Li is also present, presumably from EC and TEP reduction and graphite exfoliation. This peak also grows increasingly complex with higher TEP content, beginning at higher onset potentials and splitting into multiple overlapping peaks with 50% and 100% TEP.

### Solvation Behaviour

The co-intercalating behaviour of solvents, like organophosphates, is closely linked to their strong Li<sup>+</sup> ion solvation,<sup>[27,28]</sup> which can make the de-solvation of Li<sup>+</sup> ions at the graphite interface energetically unfavourable. It is well-established that

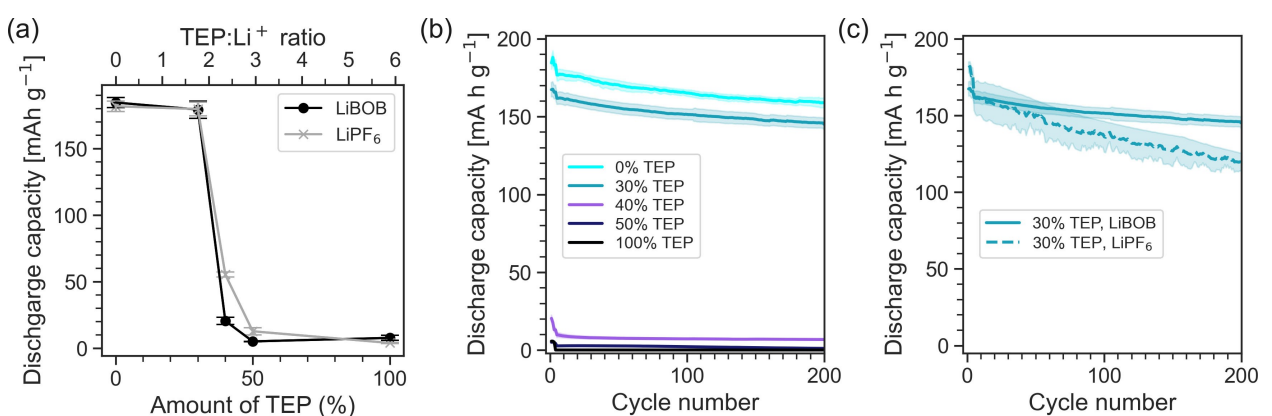


**Figure 1.** (a) 1<sup>st</sup>-cycle discharge capacities at a C-rate of C/10 plotted against the TEP content in the electrolyte. Each data point represents the mean of 3–5 cells. (b) Cycling performance of NMC | graphite cells with LiBOB-containing electrolytes in 0, 30, 40 and 50% TEP at a C-rate of C/5. (c) Comparison of cycling performance of 30% TEP electrolytes with LiBOB and LiPF<sub>6</sub> salts at a C-rate of C/5. The error bars in (a) and the shaded regions in (b)–(c) represent the standard errors.

$\text{Li}^+$  ions are preferentially coordinated by phosphates over carbonate esters. For example, according to NMR data, even at a relatively low TMP content of 25%, 95% of the TMP in an electrolyte containing TMP, EC, DEC and  $\text{LiPF}_6$  is coordinated to  $\text{Li}^+$ , compared to 19% and 25% of the DEC and EC, respectively. Conversely, at 25% total carbonate content, only 10% and 7% of the DEC and EC are coordinated to  $\text{Li}^+$ , respectively.<sup>[29]</sup> (The coordination ratios of the components with  $\text{Li}^+$  can be obtained through diffusion-ordered NMR spectroscopy (DOSY), which is described in more detail in reference 29.) Electrolytes containing TEP, EC and  $\text{LiPF}_6$  show similar trends of preferential  $\text{Li}^+$  coordination by TEP.<sup>[17]</sup>  ${}^7\text{Li}$ ,  ${}^{31}\text{P}$  and  ${}^{13}\text{C}$  NMR analysis of the LiBOB+TEP/[EC:EMC] electrolytes used in the present work show the same trends (Figure 2). In general, an upfield-shifted signal (that is, one shifted to a lower energy) indicates higher electron density around the atom in question, while a down-field-shifted signal indicates lower electron density. The  ${}^7\text{Li}$  signal continuously shifts upfield with increasing TEP content (Figure 2a). This indicates higher electron density around the  $\text{Li}^+$  ions, an effect of the TEP molecules' higher coordination strength. Conversely, the  ${}^{31}\text{P}$  signal of the TEP molecules is downfield shifted with increasing TEP content, as electron density is localized away from the phosphorus atoms into the  $\text{P}=\text{O}-[\text{Li}^+]$  interaction. The  ${}^{13}\text{C}$  signal of the bis(oxalate borate) anion (Figure 2c, left) shifts upfield with increasing TEP content, which is also consistent with the trend of increased TEP- $\text{Li}^+$  coordination at the expense of all other  $\text{Li}^+$  interactions. Finally, the  ${}^{13}\text{C}$  signals of the EC and EMC molecules (Figure 2c, right) shift downfield with increasing TEP content as more TEP

molecules and fewer EC and EMC molecules are coordinated to  $\text{Li}^+$ . Tellingly, at 50% TEP, the signals are closer to that of "free" EC and EMC than to that of the 30% TEP electrolyte.

### Electrolyte Decomposition

At standard  $\text{Li}^+$  concentrations of ca. 1 M, an SEI is formed primarily from the decomposition products of solvent molecules coordinated to  $\text{Li}^+$  ions.<sup>[30]</sup> In conventional electrolytes, EC is a key SEI-forming compound because it coordinates  $\text{Li}^+$  preferentially compared with most other electrolyte components.<sup>[31]</sup> To study the SEI formation processes, we tracked the gaseous decomposition products of electrolytes containing 0%, 30%, 50%, 100% TEP solvent using an online electrochemical mass spectrometry (OEMS) technique developed by Lundström and Berg.<sup>[22]</sup> To simplify the mass spectra, the EMC solvent was replaced with diethyl carbonate (DEC). The generation of a selection of gases was measured on dedicated mass-to-charge ratio ( $m/z$ ) channels. The gases with  $m/z=26$  (a component of the fragmentation patterns of both  $\text{C}_2\text{H}_4$  and  $\text{C}_2\text{H}_6$ ) and 44 ( $\text{CO}_2$ ) will primarily be discussed.  $\text{C}_2\text{H}_4$  is a common byproduct of the reduction of EC on graphite,<sup>[32–34]</sup> while  $\text{C}_2\text{H}_6$  is a byproduct of TEP decomposition (Figure S4).  $\text{CO}_2$  is the detected byproduct of EC side reactions (for example with  $\text{OH}^-$  from residual  $\text{H}_2\text{O}$ )<sup>[35]</sup> and BOB<sup>-</sup> reduction.<sup>[36]</sup>

The electrolytes containing 50% and 100% TEP solvent exhibited significantly more gas evolution than those with no TEP and 30% TEP (Figure 3a and Table 1).  $\text{C}_2\text{H}_6$  was the most

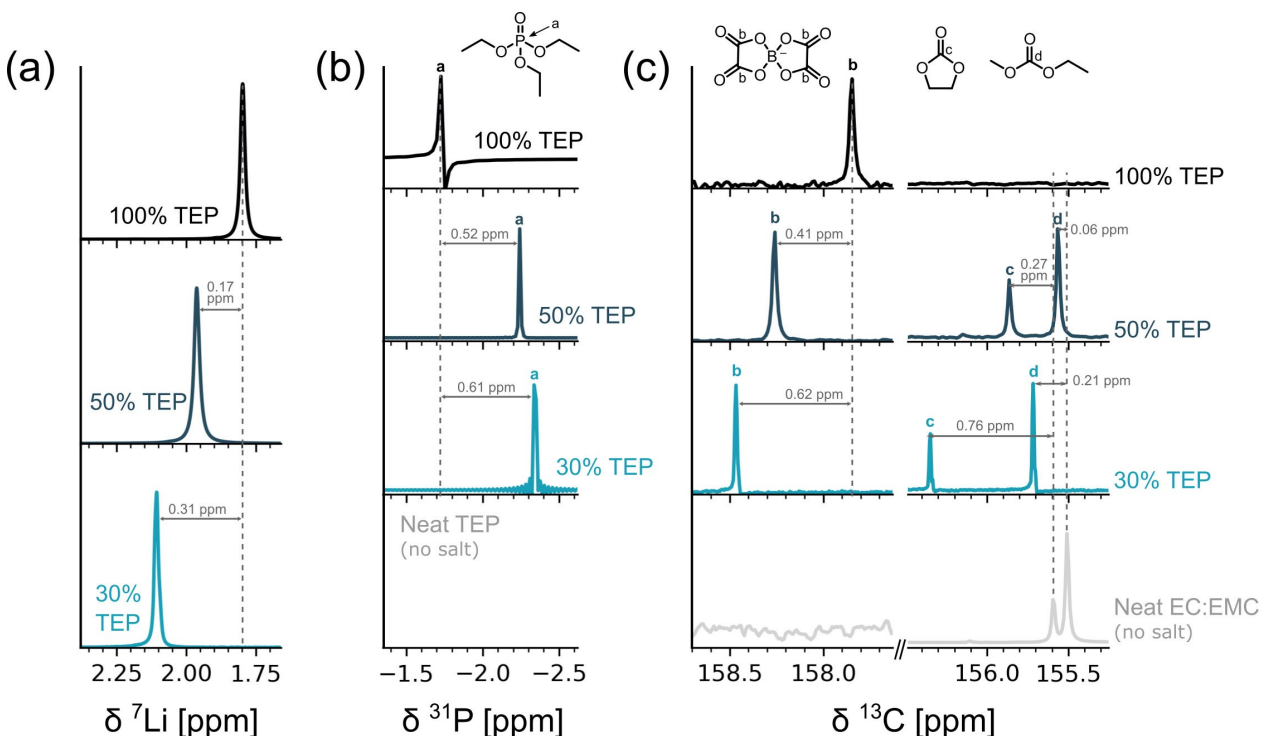


**Figure 2.** (a)  ${}^7\text{Li}$  NMR spectra of electrolytes containing 30%–100% TEP solvent; (b)  ${}^{31}\text{P}$  NMR spectra of neat TEP and electrolytes containing 30%–100% TEP solvent; (c)  ${}^{13}\text{C}$  NMR spectra of neat EC:EMC (7:3) and electrolytes containing 30%–100% TEP solvent. Note: the NMR spectra of the electrolyte containing 0% TEP solvent is not shown, as its chemical shifts are not comparable to the others due to its different  $\text{Li}^+$  concentration (0.7 M instead of 1 M).

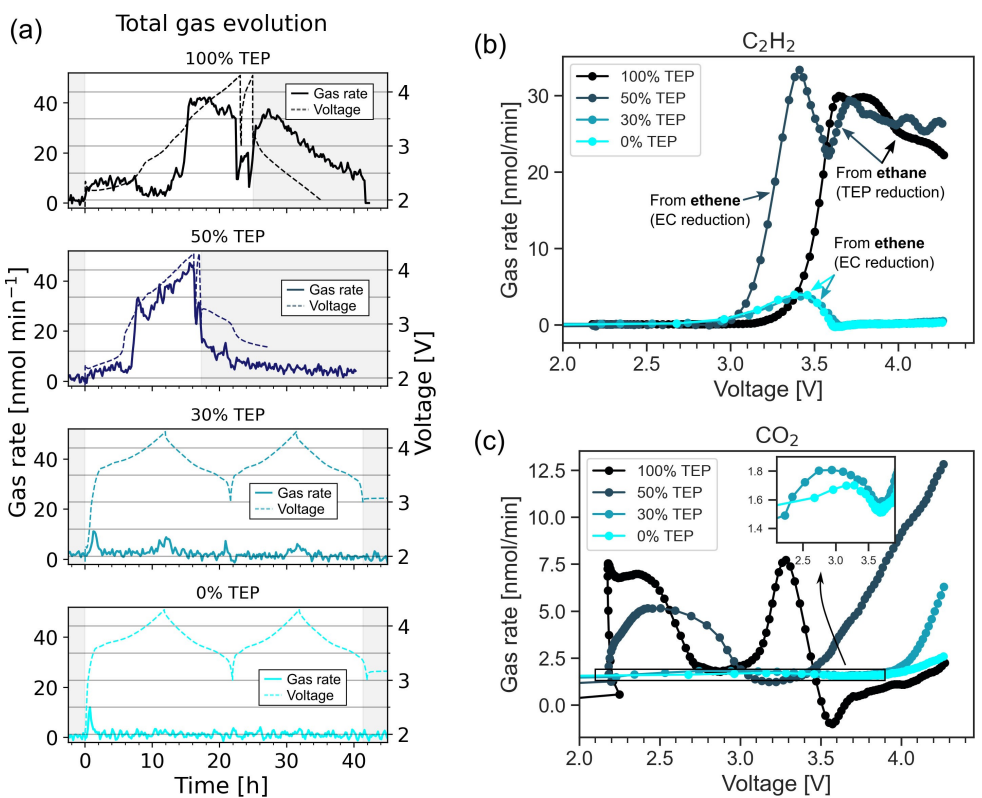


**Figure 3.** (a) total evolution rates of all m/z channels monitored and voltage profiles for electrolytes containing TEP/[EC:DEC] mixtures containing 0%, 30%, 50% and 100% TEP. The shaded regions indicate rest periods (i.e., when no current is applied). (b)–(c) evolution rates for C<sub>2</sub>H<sub>4</sub>/C<sub>2</sub>H<sub>6</sub> and CO<sub>2</sub>. In the inset in (c), the data for 100% and 50% have been left out to improve readability.

**Table 1.** Total gas evolution in mmol and as a multiple of gas evolution from 0% TEP, measured by pressure increase in the cell.

TEP content in electrolyte	Total gas evolution over 2 charge-discharge cycles	Total gas evolution, normalized to 0% TEP
0%	7.6 mmol	1
30%	8.6 mmol	1.1
50%	29.3 mmol	3.9
100%	40.3 mmol	5.3

significant gas detected in both cases (Figure 3b). The 50% TEP electrolyte also displayed a significant amount of C<sub>2</sub>H<sub>4</sub> evolution, as is common with EC-containing electrolytes, where it originates from EC reduction on graphite. However, we found that TEP reduction chiefly produces ethane, not ethene (Figure S4). The m/z=26 signal detected from the TEP-free electrolyte in Figure 3b can be ascribed to EC reduction and C<sub>2</sub>H<sub>4</sub> evolution. This is most likely also the case for the 30% TEP electrolyte, as its m/z=26 peak is almost identical in shape and intensity. The much larger m/z=26 peaks of 100% TEP electrolyte, however, are due primarily to ethane evolution from TEP decomposition.

For the 50% TEP electrolyte, two sets of m/z=26 peaks were observed. The first peak, between 3 and 3.6 V, is similar to the one in the TEP-free electrolyte, but much more intense. The second set is a series of large, overlapping peaks at 3.6–4.3 V, at the same voltage and with a similar shape as the TEP reduction

peak from the 100% TEP electrolyte. These observations suggest that in the 50% TEP electrolyte, EC reduction still takes place, but the SEI formed is not electronically insulating enough to prevent further reduction. In other words, the solvent is decomposed until it is used up (or until the overpotential causes the cell to reach its voltage limit). This could be an effect of the very low EC-Li<sup>+</sup> coordination in this electrolyte, which could potentially alter the nature of the decomposition products significantly.

The electrolytes show significant but highly variable CO<sub>2</sub> evolution (Figure 3c), much of which likely originates from the decomposition, both reductive<sup>[37]</sup> and oxidative,<sup>[36]</sup> of the BOB<sup>-</sup> anion, and EC side reactions with OH<sup>-</sup>. As with the m/z=26 peaks, CO<sub>2</sub> evolution is much more significant for the 100% and 50% TEP electrolytes, indicating significant BOB<sup>-</sup> decomposition. However, CO<sub>2</sub> generation in LIBs is often the result of complex reactions or subject to delayed observation. One example of this is that CO<sub>2</sub>-producing reactions often coexist with CO<sub>2</sub>-consuming reactions.<sup>[38,39]</sup> Another is that the slow diffusion of residual H<sub>2</sub>O through the SEI can generate OH<sup>-</sup>, which reacts with EC to form poly(ethylene glycol) and CO<sub>2</sub>, causing CO<sub>2</sub> evolution to be observed well beyond the normal onset potential of this reaction.<sup>[34]</sup> For this reason, the CO<sub>2</sub> evolution will not be interpreted further in this work.

## Electrode Surface Analysis

Synchrotron-based energy-tuned X-ray photoelectron spectroscopy was employed to investigate the surface chemistry of the graphite electrodes after cycling in electrolytes with various TEP contents, to further understand the decomposition processes of the electrolyte. C 1s core level spectra are presented in Figure 4. For the pristine electrode, the peak with the highest relative intensity (~284 eV) corresponds to the C=C bonding environment in the graphite active material. Other species, which are most prominent in the more surface-sensitive measurement (200 eV KE), likely correspond to the binder (sodium carboxymethyl cellulose—NaCMC, and styrene-butadiene—SBR; a signal for Na 2s from NaCMC is shown in Figure S5a). C—O and C=O environments for the binder are also observed in the O 1s spectra of the pristine electrode (Figure S5b). In the 0% TEP (EC-EMC) electrolyte case, peaks for bonding environments that correspond to species typically associated with the SEI from a carbonate electrolyte are observed. These include C—O at ~286 eV and inorganic carbonates ( $\text{Li}_2\text{CO}_3$ ) at ~290 eV<sup>[40]</sup> as the

main components. The  $-\text{CO}_2-$  species (~288.5 eV) are likely lithium oxalate formed by  $\text{BOB}^-$  reduction.<sup>[37]</sup> It is also observed that the relative intensity of the graphite peak has dropped substantially as the SEI forms the surface region of the sample, preventing escape of electrons from the bulk electrode material. As expected, the relative intensity of the graphite peak increases with greater probing depths and is most noticeable at 7.05 keV photon energy. With 30% TEP, a significantly larger degree of carbonate formation is observed, this time also with the presence of a peak corresponding to polycarbonates (~291 eV<sup>[40]</sup>), which have been proposed to form via both radical and ionic propagation mechanisms.<sup>[41,42]</sup> Interestingly, the relative intensity of the polycarbonate peak increases with probing depth, suggesting that this species is not very present at the surface, but more so deeper into the SEI layer. For this sample, the largest absolute intensity is observed at the surface in Li 1s and B 1s spectra (Figure S7a,b), indicating a notable presence of LiBOB or its decomposition products, which concurs with the  $\text{CO}_2$  evolution observed in gas analysis experiments. Similar to that for the 0% TEP, there is little signal for graphite in the

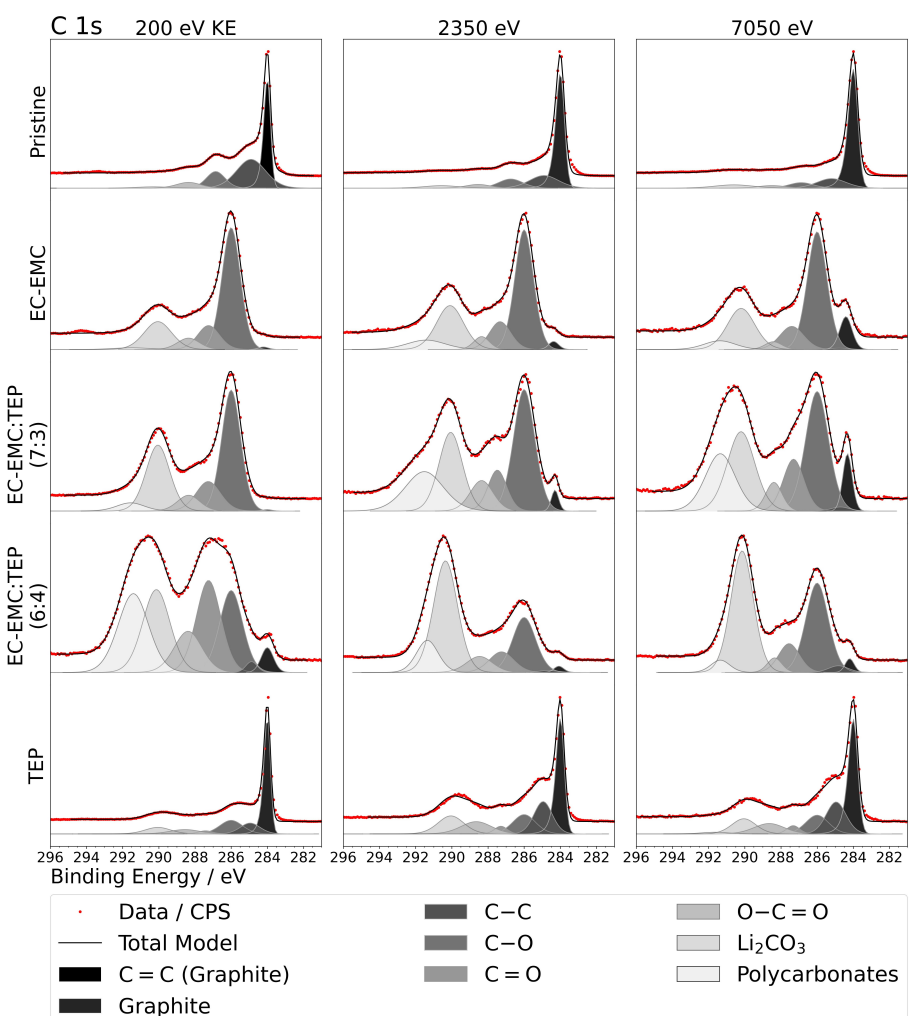


**Figure 4.** X-ray photoelectron spectra for the C 1s core level measured for pristine graphite electrodes as well as from cells (against NMC622 cathodes) fully charged to 4.3 V. 0%, 30%, 40%, and 100% TEP electrolytes were investigated. Three photon energies were used to probe different depths of the sample surface: a soft X-ray beam with photon energy (eV) corresponding to 200 eV kinetic energy-KE (3 nm), and hard X-rays with photon energies of 2.35 keV (18 nm) and 7.05 keV (50 nm).

most surface-sensitive measurement, but it is observed at higher energies.

For the 40% TEP, some quite significant changes begin to occur. The SEI can be said to be much richer in carbonate species, with the  $\text{Li}_2\text{CO}_3$  peak being the most intense peak in the spectra at the two greater probing depths, compared with C–O previously. At the very surface, there are many dominant species, including C–O, C=O,  $\text{Li}_2\text{CO}_3$  and polycarbonates. Furthermore, a significant shift in the corresponding spectra for O 1s (Figure S5b) and P 2p (Figure S6a), as well as the highest absolute intensity of P and O (Figure S7c, Figure S8), suggests a surface rich in phosphates. The most noteworthy observation is the presence of the graphite peak with some intensity at all three probing depths. In particular, to observe this peak in the most surface-sensitive measurement, and with greater relative intensity than for the more bulk measurements, can only suggest that there are bare graphitic surfaces exposed on the sample, despite the seemingly complex SEI chemistry also being present. With a homogeneous SEI layer with full coverage, one would expect a lower relative intensity for the surface measurement than for the higher energy measurements. These exposed graphite particles may be as a result of an inhomogeneous formation of the SEI, a breakup or delamination of the SEI, perhaps as a result of high voltage processes, or a pronounced change in the structure of the electrode material resulting in its exposure. As observed for the 100% TEP case, it is suspected to be the latter scenario that is responsible for this. The use of the 100% TEP-based electrolyte results in a very high relative intensity signal for graphite in the measurements for all three probing depths. The components of the SEI, including carbonates and other carbon-oxygen species, such as those observed in the cases with lower TEP content, are still present in the spectra. As was observed for the gas analysis, it is expected that the decomposition of the LiBOB plays a significant role here,

with a relatively high B 1s signal being observed at the surface (Figure S7b);  $\text{Li}_2\text{CO}_3$  is a known product of LiBOB reduction, alongside oligoborates and  $\text{Li}_2\text{C}_2\text{O}_4$ .<sup>[37]</sup> In addition, the B 1s signals appear with higher relative intensity at greater probing depths, while the graphite has a higher relative intensity (and absolute intensity relative to the pristine electrode; see Figure S9) at the most surface-sensitive probing depth. This observation is highly consistent with extensive exfoliation of the graphite particles, revealing a large extent of exposed graphite surfaces and with low intensity for other species.

Taken together, the NMR, OEMS and XPS results, which are summarized schematically in Figure 5, help explain the “threshold effect” observed with the irreversible capacities of graphite in TEP-based electrolytes. With increasing TEP content, TEP molecules increasingly dominate the solvation of  $\text{Li}^+$ . 30 vol% represents an inflection point above which the electrolyte appears to contain insufficient carbonate ester-solvated  $\text{Li}^+$  for protective SEI formation and reversible  $\text{Li}^+$  transport. The resulting intercalation of TEP- $\text{Li}^+$  species into the graphite results in the exfoliation of the electrode, accompanied by decomposition of the TEP and extensive ethane gas formation. While both the OEMS and the XPS data indicate the presence of conventional EC reduction and EC-derived SEI products even in the exfoliated electrodes, these are clearly either unable to prevent TEP co-intercalation, or form after the electrode is already exfoliated.

Some co-intercalating solvents, such as propylene carbonate, can be stabilized in graphite-containing cells using additives. Using the 40% TEP electrolyte as a base electrolyte, we tested three additives commonly employed to prevent co-intercalation: vinyl ethylene carbonate (VEC),<sup>[43]</sup> 1,3,2-dioxathiolane-2,2-dioxide (DTD)<sup>[44]</sup> and ethylene sulfite (ES).<sup>[45]</sup> None of these succeeded in enabling anything close to the full capacity of the NMC622|graphite cells (Figure S10). However, with 5%

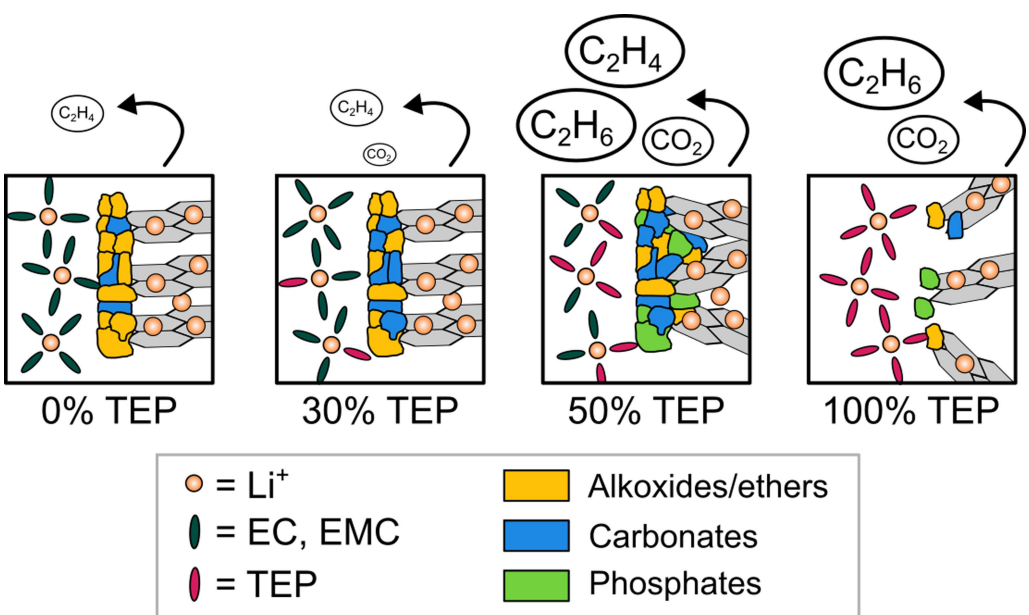


**Figure 5.** Schematic summary of the effects of TEP at various concentrations on the  $\text{Li}^+$  solvation shell, SEI formation and gas generation of carbonate ester-based electrolytes.

ES, the initial discharge capacity was ca.  $50 \text{ mAhg}^{-1}$  – a significant improvement that suggests TEP yet may be rendered usable with graphite anodes with the right combination and concentration of additives. TEP's high polarity compared to carbonate esters could in particular be exploited to use additives that are not otherwise soluble, such as lithium nitrate.<sup>[46]</sup>

## Conclusions

TEP is a non-flammable electrolyte solvent whose tendency to co-intercalate into graphite currently holds it back from use in batteries. In this work, the electrochemical behaviour of TEP electrolytes mixed with 3:7 EC:EMC, and employing the fluorine-free salt LiBOB, was tested at TEP contents of 0%, 30%, 40%, 50% and 100%. A sharp decline in the reversibility of  $\text{Li}^+$  intercalation into graphite between 30 and 40% TEP content was confirmed: at 30%, the cells achieve nearly the same reversible capacity as at 0% and exhibit stable cycling, while at 40% the reversible capacity is close to zero. A plausible explanation for this is that, above 30% TEP content, there is insufficient "TEP-free"  $\text{Li}^+$  to form an SEI, although further research is needed to confirm this hypothesis. NMR analysis of a selection of the electrolytes, combined with previously reported solvation data of  $\text{Li}^+$  solutions in alkyl phosphates, confirm that  $\text{Li}^+$  exhibits a strong preference for solvation by TEP over EC, EMC and the bis(oxalato)borate anion. *Operando* mass spectrometry of the gases generated by these electrolytes also show that, at 30% TEP content, no detectable decomposition of TEP takes place, while at higher TEP contents, significant ethane generation from TEP decomposition is observed. Surprisingly, even the EC and bis(oxalato)borate anion appear to decompose to an extent in the 40%, 50% and 100% TEP electrolytes, even forming detectable SEI layers, according to X-ray photoelectron spectroscopy. However, the SEI in such cases is not electronically insulating enough to protect the graphite anode from continued reaction with the electrolyte. XPS depth profiling reveals some significant changes in the surface layer composition on graphite with a TEP content greater than 30%, particularly with detection of graphitic carbon even at shallow probing depths. This agrees well with the observed exfoliation of graphite by TEP co-intercalation, rendering those electrolytes with higher TEP contents unable to form a stable surface layer. This work has demonstrated the challenges associated with employing safer electrolytes, which often do not passivate the electrode surfaces well and decompose during cycling. Further strategies are required to prevent the co-intercalation of TEP, possibly through tuning of the electrolyte composition and solvation structure or by employing electrode surface modifications. Enabling an even higher TEP content than 30% in the electrolyte with high capacity and stable cycling would most likely bring further safety benefits. Finally, TEP's ability to fully dissolve LiBOB at standard battery electrolyte concentrations represents an interesting and under-appreciated benefit of the solvent and merits more dedicated consideration. For example,

the reduced toxicity and environmental footprint of this fluorine-free electrolyte could be studied.

## Supporting Information Summary

Supporting Information Available: a document containing additional graphs on internal cell resistance, coulombic efficiency, cyclic voltammograms, gas evolution rates, XPS data, and the effect of various additives on EC:EMC + 40% TEP.

## Abbreviations

BOB	Bis(oxalato)borate
DEC	Diethyl carbonate
EC	Ethylene carbonate
EMC	Ethyl methyl carbonate
HAXPES	Hard X-ray photoelectron spectroscopy
NMC622	$\text{LiNi}_{0.6}\text{Mn}_{0.2}\text{Co}_{0.2}\text{O}_2$
NMR	Nuclear magnetic resonance
OEMS	Online electrochemical mass spectrometry
SEI	Solid electrolyte interphase
SOXPES	Soft X-ray photoelectron spectroscopy
TEP	Triethyl phosphate
XPS	X-ray photoelectron spectroscopy

## Acknowledgements

The authors acknowledge financial support from the Swedish Energy Agency (projects P2021-90019 and P2022-00045). This work forms part of the Swedish strategic research programme StandUp for Energy. This work was carried out with the support of Diamond Light Source, instrument I09 (proposal SI31857).

## Conflict of Interests

The authors declare no conflict of interest.

## Data Availability Statement

The data that support the findings of this study are available from the corresponding author upon reasonable request.

**Keywords:** Lithium-ion battery · Non-flammable electrolyte · Electrolyte decomposition · Solid electrolyte interphase · Electrochemistry · Interfaces

[1] K. Brandt, J. Schultheiß, M. Schweizer-Berberich, Chapter 8B - Managing of Risk by Battery Manufacturers. In *Electrochemical Power Sources: Fundamentals, Systems, and Applications*; J. Garche, K. Brandt, Eds.; Elsevier, 2019; pp 303–335. <https://doi.org/10.1016/B978-0-444-63777-2.00008-6>.

- [2] B. Y. Liaw, F. Wang, Y. Wei, Chapter 8 A - Managing of Risk by Cell Manufacturers. In *Electrochemical Power Sources: Fundamentals, Systems, and Applications*; J. Garche, K. Brandt, Eds.; Elsevier, 2019; pp 269–302. <https://doi.org/10.1016/B978-0-444-63777-2.00008-6>.
- [3] K. Brandt, J. Garche, Chapter 1 - General Battery Safety Considerations. In *Electrochemical Power Sources: Fundamentals, Systems, and Applications*; J. Garche, K. Brandt, Eds.; Elsevier, 2019; pp 1–19. <https://doi.org/10.1016/B978-0-444-63777-2.00001-3>.
- [4] F. Gebert, M. Longhini, F. Conti, A. J. Naylor, *J. Power Sources* **2023**, *556*, 232412.
- [5] M. Balaish, J. C. Gonzalez-Rosillo, K. J. Kim, Y. Zhu, Z. D. Hood, J. L. M. Rupp, *Nat. Energy* **2021**, *6*(3), 227–239.
- [6] N. J. Taylor, J. Sakamoto, *Am. Ceram. Soc. Bull.* **2019**, *98*(7), 26–31.
- [7] J. Kasemchainan, P. G. Bruce, *Johns. Matthey Technol. Rev.* **2018**, *62*(2), 177–180.
- [8] E. Jónsson, *Energy Storage Mater.* **2020**, *25*, 827–835.
- [9] J. W. Haste, *J. Res. Natl. Bur. Stand. Sect. Phys. Chem.* **1973**, *77* A(6), 733–754.
- [10] H. Nakagawa, M. Ochida, Y. Domi, T. Doi, S. Tsubouchi, T. Yamanaka, T. Abe, Z. Ogumi, *J. Power Sources* **2012**, *212*, 148–153.
- [11] W. W. A. van Ekeren, M. Albuquerque, G. Ek, R. Mogensen, W. R. Brant, L. T. Costa, D. Brandell, R. Younesi, *J. Mater. Chem. A* **2023**, *11*(8), 4111–4125.
- [12] P. Murmann, X. Mönnighoff, N. von Aspern, P. Janssen, N. Kalinovich, M. Shevchuk, O. Kazakova, G.-V. Röschenthaler, I. Čekić-Lasković, M. Winter, *J. Electrochem. Soc.* **2016**, *163*(5), A751.
- [13] X. Mönnighoff, P. Murmann, W. Weber, M. Winter, S. Nowak, *Electrochim. Acta* **2017**, *246*, 1042–1051.
- [14] X. X. Cao, Y. Xu, L. Zhang, M. H. Engelhard, L. Zhong, X. Ren, H. Jia, B. Liu, C. Niu, B. E. Matthews, H. Wu, B. W. Arey, C. Wang, J.-G. Zhang, W. Xu, *ACS Energy Lett.* **2019**, *4*(10), 2529–2534.
- [15] K. Xu, M. S. Ding, S. Zhang, J. L. Allen, T. R. Jow, *J. Electrochem. Soc.* **2002**, *149*(5), A622.
- [16] Z. Zeng, V. Murugesan, K. S. Han, X. Jiang, Y. Cao, L. Xiao, X. Ai, H. Yang, J.-G. Zhang, M. L. Sushko, J. Liu, *Nat. Energy* **2018**, *3*(8), 674–681.
- [17] M. Liu, Z. Zeng, C. Gu, F. Ma, Y. Wu, Q. Wu, X. Yang, X. Chen, S. Cheng, J. Xie, *ACS Energy Lett.* **2024**, *9*(1), 136–144.
- [18] M. J. Lacey, *ChemElectroChem* **2017**, *4*(8), 1997–2004.
- [19] Z. Geng, T. Thiringer, M. J. Lacey, *IEEE Trans. Transp. Electrif.* **2022**, *8*(2), 2985–2995.
- [20] C. J. Powell, A. A. Jablonski, NIST Electron Inelastic-Mean-Free-Path Database, version 1.2; SRD 71; National Institute of Standards and Technology: Gaithersburg, MD, 2010. (accessed 2023-11-27).
- [21] S. Tanuma, C. J. Powell, D. R. Penn, *Surf. Interface Anal.* **1994**, *21*(3), 165–176.
- [22] R. Lundström, E. J. Berg, *J. Power Sources* **2021**, *485*, 229347.
- [23] S. Kannan, K. Kishore, *J. Chem. Eng. Data* **1999**, *44*(4), 649–655.
- [24] E. R. Logan, E. M. Tonita, K. L. Gering, L. Ma, M. K. G. Bauer, J. Li, L. Y. Beaulieu, J. R. Dahn, *J. Electrochem. Soc.* **2018**, *165*(3), A705.
- [25] M. E. Spahr, T. Palladino, H. Wilhelm, A. Würsig, D. Goers, H. Buqa, M. Holzapfel, P. Novák, *J. Electrochem. Soc.* **2004**, *151*(9), A1383.
- [26] K. Xu, S. S. Zhang, U. Lee, J. L. Allen, T. R. Jow, *J. Power Sources* **2005**, *146*(1), 79–85.
- [27] Y. Yamada, Y. Koyama, T. Abe, Z. Ogumi, *J. Phys. Chem. C* **2009**, *113*(20), 8948–8953.
- [28] M. Qin, Z. Zeng, Q. Wu, H. Yan, M. Liu, Y. Wu, H. Zhang, S. Lei, S. Cheng, J. Xie, *Energy Environ. Sci.* **2023**, *16*(2), 546–556.
- [29] B. Ernould, L. Sieuw, G. Barozzino-Consiglio, J.-F. Gohy, A. Vlad, *ACS Appl. Energy Mater.* **2019**, *2*(11), 7879–7885.
- [30] K. Xu, Y. Lam, S. S. Zhang, T. R. Jow, T. B. Curtis, *J. Phys. Chem. C* **2007**, *111*(20), 7411–7421.
- [31] A. von Cresce, K. Xu, *Electrochem. Solid-State Lett.* **2011**, *14*(10), A154.
- [32] D. Aurbach, Y. Ein-Ely, A. Zaban, *J. Electrochem. Soc.* **1994**, *141*(1), L1–L3.
- [33] H. Yoshida, T. Fukunaga, T. Hazama, M. Terasaki, M. Mizutani, M. Yamachi, *J. Power Sources* **1997**, *68*(2), 311–315.
- [34] R. Lundström, N. Gogoi, X. Hou, E. J. Berg, *J. Electrochem. Soc.* **2023**, *170*(4), 040516.
- [35] M. Metzger, B. Strehle, S. Solchenbach, H. A. Gasteiger, *J. Electrochem. Soc.* **2016**, *163*(7), A1219.
- [36] M. Xu, N. Tsiovaras, A. Garsuch, H. A. Gasteiger, B. L. Lucht, *J. Phys. Chem. C* **2014**, *118*(14), 7363–7368.
- [37] B. S. Parimalam, B. L. Lucht, *J. Electrochem. Soc.* **2018**, *165*(2), A251–A255.
- [38] D. Aurbach, Y. Ein-Ely, O. Chusid (Youngman), Y. Carmeli, M. Babai, H. Yamin, *J. Electrochem. Soc.* **1994**, *141*(3), 603.
- [39] R. Bernhard, M. Metzger, H. A. Gasteiger, *J. Electrochem. Soc.* **2015**, *162*(10), A1984.
- [40] V. Shutthanandan, M. Nandasiri, J. Zheng, M. H. Engelhard, W. Xu, S. Thevuthasan, V. Murugesan, *J. Electron Spectrosc. Relat. Phenom.* **2019**, *231*, 2–10.
- [41] H. H. Tavassol, J. W. Butthker, G. A. Ferguson, L. A. Curtiss, A. A. Gewirth, *J. Electrochem. Soc.* **2012**, *159*(6), A730–A738.
- [42] I. A. Shkrob, Y. Zhu, T. W. Marin, D. Abraham, *J. Phys. Chem. C* **2013**, *117*(38), 19255–19269.
- [43] Y. Hu, W. Kong, H. Li, X. Huang, L. Chen, *Electrochim. Commun.* **2004**, *6*(2), 126–131.
- [44] P. Janssen, R. Schmitz, R. Müller, P. Isken, A. Lex-Balducci, C. Schreiner, M. Winter, I. Čekić-Lasković, R. Schmitz, *Electrochim. Acta* **2014**, *125*, 101–106.
- [45] M. D. Bhatt, C. O'Dwyer, *J. Electrochem. Soc.* **2014**, *161*(9), A1415.
- [46] Y. Quan, X. Cui, M. Wang, L. Hu, D. Zhao, N. Zhang, F. Zhang, S. Li, *Chem. Eng. J.* **2024**, *489*, 151539.

Manuscript received: May 27, 2024

Revised manuscript received: July 12, 2024

Accepted manuscript online: July 15, 2024

Version of record online: September 5, 2024